

## Random sequential adsorption on partially covered surfaces

Zbigniew Adamczyk and Paweł Weroński

Citation: *The Journal of Chemical Physics* **108**, 9851 (1998); doi: 10.1063/1.476423

View online: <http://dx.doi.org/10.1063/1.476423>

View Table of Contents: <http://scitation.aip.org/content/aip/journal/jcp/108/23?ver=pdfcov>

Published by the [AIP Publishing](#)

---

### Articles you may be interested in

[The effect of impurities on jamming in random sequential adsorption of elongated objects](#)

*J. Chem. Phys.* **124**, 054713 (2006); 10.1063/1.2161206

[Irreversible adsorption of hard spheres at random site \(heterogeneous\) surfaces](#)

*J. Chem. Phys.* **116**, 4665 (2002); 10.1063/1.1446425

[Adsorption of random copolymers: A scaling analysis](#)

*J. Chem. Phys.* **110**, 2727 (1999); 10.1063/1.477996

[Extended series expansions for random sequential adsorption](#)

*J. Chem. Phys.* **108**, 3010 (1998); 10.1063/1.475687

[Fluctuations in the random sequential adsorption of disks and parallel squares: Finite size effects at low coverages](#)

*J. Chem. Phys.* **106**, 4196 (1997); 10.1063/1.473138

---



# Random sequential adsorption on partially covered surfaces

Zbigniew Adamczyk<sup>a)</sup> and Paweł Weroński

*Institute of Catalysis and Surface Chemistry, Polish Academy of Sciences, 30-239 Cracow, ul.Niezapominajek 1, Poland*

(Received 24 October 1997; accepted 11 March 1998)

The random sequential adsorption (RSA) approach was used to analyze adsorption of hard spheres at surfaces precovered with smaller sized particles. Numerical simulations were performed to determine the available surface fraction  $\phi_l$  of larger particles for various particle size ratios  $\lambda = a_l/a_s$  and surface concentration of smaller particles  $\theta_s$ . It was found that the numerical results were in a reasonable agreement with the formula stemming from the scaled particle theory with the modification for the sphere/sphere geometry. Particle adsorption kinetics was also determined in terms of the RSA simulations. By extrapolating the  $\theta_l$  vs  $\tau^{-1/2}$  dependencies, the jamming concentrations of larger spheres  $\theta_l^\infty$  were determined as a function of the initial smaller sphere concentration. It was found that  $\theta_l^\infty$  were considerably reduced by the presence of smaller sized particles, especially for  $\lambda \gg 1$ . The pair correlation function  $g$  of larger particles in the jamming state was also determined, showing more short range ordering (at the same  $\theta_l$ ) in comparison with monodisperse systems. The theoretical predictions stemming from our calculations suggest that the presence of trace amounts of very small particles may exert a decisive influence on adsorption of larger particles. © 1998 American Institute of Physics. [S0021-9606(98)50923-3]

## INTRODUCTION

The random sequential adsorption (RSA) is one of the simplest and most efficient approaches to analyze sequences of irreversible events. In this process objects (particles) of various geometrical shape are added randomly, one at a time, to a  $D$ -dimensional volume. Once an empty space element is found the particle is permanently fixed (with no consecutive motion allowed). Otherwise it is rejected and a new addition attempt is undertaken, uncorrelated with previous attempts. The process usually starts from an empty volume and continues until the jamming state is reached when no additional object (of the same size and shape) can be added. Exact solutions of the RSA problem exist for one-dimensional problems only.<sup>1,2</sup> For higher dimensionality abundant numerical studies exist<sup>3-9</sup> in which kinetics of the RSA processes and jamming concentrations were determined in *ab initio*-type calculations. These results obtained for monodisperse spherical particles proved useful for interpreting irreversible adsorption phenomena of macromolecules, proteins, and colloid particles.<sup>10,11</sup>

However, for a broad range of practical situations this classical RSA model seems inadequate, especially for processes when polydisperse suspensions or mixtures are occurring, e.g., colloid/polymer, colloid/colloid, or protein/surfactant. Due to their higher diffusivity and concentration, the smaller sized particles will first adsorb at the interface, forming a layer which may exert a significant influence on consecutive adsorption of larger particles. Similar problems may appear in model experiments concerning colloid particle or protein adsorption when the usual cleaning procedure may

produce a layer of contamination at the substrate surface difficult to detect. This is expected to affect adsorption kinetics in the proper experiments. Hence, the subject of particle adsorption at partially covered surfaces seems attractive from a practical viewpoint.

The studies on RSA processes at covered surfaces, are also attractive theoretically in view of the limited literature on this subject. The existing works were concerned with the related problem of polydisperse disk adsorption, which is strictly two dimensional. Talbot and Schaafl<sup>12</sup> performed an approximate analysis of adsorption of two-component (bimodal) mixtures of disks widely differing in diameter. Adsorption kinetics and the jamming concentrations of larger disks were determined in the limit when the size of the smaller disk decreased to zero. In the case of spheres they were unable to find the proper jamming limit.

Meakin and Jullien<sup>13</sup> performed extensive simulations of adsorption kinetics and jamming limit for polydisperse disk mixtures characterized by bimodal, uniform, and truncated Gaussian distributions.

The quasi-three-dimensional problem of polydisperse sphere adsorption was treated in Ref. 14. However, the numerical simulations performed for hard and soft spheres according to the RSA model, were confined to suspensions characterized by narrow size distributions, i.e., 0%–20% only.

In this paper we report numerical simulations concerning adsorption of larger spheres at surfaces precovered with significantly smaller spheres. Adsorption kinetics, jamming coverages, and radial distribution function of large particles will be determined.

The problem considered in our work can be treated as the extension of the classical RSA to systems characterized

<sup>a)</sup>Author to whom correspondence should be addressed. Electronic mail: ncadamcz@cyf.-kr.edu.pl

by a discontinuous change (increase) of the size of the objects added to a volume.

It should be mentioned that some preliminary results on adsorption kinetics at covered surfaces have been published in Ref. 15.

## THE SIMULATION METHOD

The simulation algorithm was similar to that used for polydisperse sphere adsorption described in Ref. 14. The simulations were carried out over a rectangular simulation plane with the usual periodic boundary conditions at its perimeter. As in previous works,<sup>6–8,13</sup> the simulation plane was divided into subsidiary square areas (cells) of the size  $\sqrt{2}a_s$  (where  $a_s$  is the radius of the smaller particle) so the center of at most one particle could lie within a particular cell. This enhanced the efficiency of the overlapping test performed at each simulation step.

The entire simulation procedure consisted of two main stages:

- (i) the simulation plane was covered with smaller sized particles to a prescribed dimensionless surface concentration (coverage)  $\theta_s = \pi a_s^2 N_s$  (where  $N_s$  is the surface density of smaller spheres), during this stage the usual RSA simulation algorithm was used;
- (ii) then the larger spheres, having the radius  $a_l$  were introduced by choosing at random their position within the simulation area; the overlapping test between larger/larger and smaller/larger particles was carried out in the latter case by considering the true three-dimensional distances between the sphere centers.

In order to simulate the kinetic runs the dimensionless adsorption time  $\tau$  was set to zero at the beginning of the second stage. In calculations  $\tau$  was defined as

$$\tau = \frac{N_{\text{att}}}{N_{\text{ch}}} = \pi \bar{a}_l^2 N_{\text{att}}, \quad (1)$$

where  $N_{\text{ch}} = (1/\pi \bar{a}_l^2)$  is the characteristic surface concentration of larger particles and  $N_{\text{att}}$  is the overall number of attempts to place larger particles.

The maximum dimensionless time attained in our simulation was about  $10^4$  which required  $10^6$ – $10^9$  simulation steps. The jamming concentrations  $\theta^\infty$  were calculated by extrapolating the results obtained for this limiting dimensionless time, assuming power law dependencies. In order to attain a sufficient accuracy, averages from many computer runs were taken.

The available surface function (ASF) for larger particles  $\phi_1$  was calculated according to the method of Schaaf and Talbot<sup>4</sup> by exploiting the definition

$$\phi_1 = \frac{p(\theta_s, \theta_l)}{p_0} = \frac{N_{\text{succ}}}{N_{\text{att}}}, \quad (2)$$

where  $p$  is the probability of adsorbing the larger particle at the surface characterized by the coverages  $\theta_s$ ,  $\theta_l$ ,  $p_0$  is the probability of adsorption at uncovered surface (assumed equal one without loss of generality) and  $N_{\text{succ}}$  is the number

of successful adsorption events performed at fixed  $\theta_s$ ,  $\theta_l$ . In practice,  $N_{\text{att}}$  was about  $10^5$  in order to attain a sufficient accuracy of  $\phi_l$ .

The pair correlation function (radial distribution function)  $g$  was determined using the definition, i.e., from the equation

$$g(\mathbf{r}) = \frac{S}{N^2} \left\langle \sum_{i=1}^N \sum_{j=1}^N \delta_D[\mathbf{r} - (\mathbf{r}_j - \mathbf{r}_i)] \right\rangle, \quad (3)$$

where  $\mathbf{r}$  is the position vector of a point over the adsorption plane (measured from the center of an adsorbed particle),  $S$  is the surface area for which the  $g$  function should be evaluated,  $N$  is total number of particles adsorbed over this area,  $\delta_D$  is the Dirac delta function,  $\mathbf{r}_i$ ,  $\mathbf{r}_j$  are the position vectors of the  $i$  and  $j$  particle, and angle brackets means the ensemble average.

In absence of external forces when the system can be treated as isotropic, the vector  $\mathbf{r}$  can be replaced by the radial coordinate  $r$  and the pair correlation function can be calculated more directly by converting Eq. (3) to the form

$$g(\mathbf{r}) = g(r) = \frac{S}{N} \frac{\bar{N}_a(r)}{2\pi r \Delta r}, \quad (4)$$

where  $\bar{N}_a(r) = (1/N) \langle N_a \rangle$  is the averaged number of particles within the annulus of the mean radius  $r$  and the thickness  $\Delta r$ .

For evaluating  $g$  the coordinates of about 20 000 particles were considered.

All calculations discussed hereafter were performed for particle size ratio  $\lambda = a_l/a_s$  of 2.2 (this was chosen to match the experimental conditions), 5 and 10.

## ANALYTICAL APPROXIMATION

Due to a lack of appropriate expressions for the available surface function in the case of RSA of large particles at precovered surfaces, we tested our results in terms of the equilibrium adsorption approaches. This seems reasonable since  $\theta_l$  at precovered surfaces is generally much smaller than for uncovered surfaces.

According to the scaling particle theory (SPT) formulated in Ref. 16 and then extended to multicomponent mixtures in Refs. 17 and 18, the equilibrium ASF functions for bimodal suspension of disks of radius  $a_1$  and  $a_2$  are given by the expressions

$$\begin{aligned} \phi_1 &= -\ln \left( \frac{\mu_1^R}{kT} \right) = (1 - \theta) \exp \left[ - \frac{3\theta_1 + (1/\gamma)(1/\gamma + 2)\theta_2}{1 - \theta} \right. \\ &\quad \left. - \left( \frac{\theta_1 + (1/\gamma)\theta_2}{1 - \theta} \right)^2 \right], \\ \phi_2 &= -\ln \left( \frac{\mu_2^R}{kT} \right) = (1 - \theta) \exp \left[ - \frac{3\theta_2 + \gamma(\gamma + 2)\theta_1}{1 - \theta} \right. \\ &\quad \left. - \left( \frac{\theta_2 + \gamma\theta_1}{1 - \theta} \right)^2 \right], \end{aligned} \quad (5)$$

where  $\mu_1^R$  and  $\mu_2^R$  are the residual potentials of the smaller and larger particles, respectively,  $\theta = \theta_1 + \theta_2$  and  $\gamma = a_2/a_1$  is the disk size ratio. It should be noted that Eq. (5) describes a two-dimensional situation only.

It seems, however, that useful approximations of the sphere adsorption problem (a quasi-three-dimensional situation) can be formulated by redefining the geometrical parameter  $\gamma$ . Thus, by expanding Eq. (5) in the power series of  $\theta$  (up to the order of two) one obtains the expression

$$\begin{aligned}\phi_1 &\cong 1 - 4\theta_1 - (1/\gamma + 1)^2 \theta_2 + 0(\theta_1 \theta_2, \theta_1^2, \theta_2^2), \\ \phi_2 &\cong 1 - 4\theta_2 - (\gamma + 1)^2 \theta_1 + 0(\theta_1 \theta_2, \theta_1^2, \theta_2^2).\end{aligned}\quad (6)$$

Now, from the general result of Widom<sup>19</sup> it can be deduced that

$$\phi_1 \cong 1 - \bar{S}_1 \theta_1 - \frac{\bar{S}_{12}}{\lambda^2} \theta_2 + 0(\theta_1 \theta_2, \theta_1^2, \theta_2^2), \quad (7)$$

$$\phi_2 \cong 1 - \bar{S}_1 \theta_2 - \bar{S}_{12} \theta_1 + 0(\theta_1 \theta_2, \theta_1^2, \theta_2^2),$$

where  $\pi a_1^2 \bar{S}_1$ ,  $\pi a_1^2 \bar{S}_{12}$ , are the exclusion areas for two smaller spheres and for the smaller/larger sphere, respectively.

From the elementary geometry one has

$$\begin{aligned}\bar{S}_1 &= 4, \\ \bar{S}_{12} &= 4\lambda.\end{aligned}\quad (8)$$

Thus, Eq. (7) can be matched with the series expansion Eq. (6) when

$$\gamma = 2\sqrt{\lambda} - 1. \quad (9)$$

Denoting  $a_1 = a_s$  and  $a_2 = a_l$  and using Eqs. (9) and (5) one can derive the analytical expression for the ASF function of larger particles at surfaces precovered with smaller particles in the form

$$\begin{aligned}\phi_l(\theta_s, \theta_l) &= (1 - \theta) \exp \left\{ - \frac{3\theta_l + (4\lambda - 1)\theta_s}{1 - \theta} \right. \\ &\quad \left. - \left[ \frac{\theta_l + (2\sqrt{\lambda} - 1)\theta_s}{1 - \theta} \right]^2 \right\} \\ &= \phi_l^0(\theta_s) \left( 1 - \frac{\theta_l}{1 - \theta_s} \right) \exp \left\{ - \frac{4(\lambda - 1)\theta_s + 3}{1 - \theta_s} \frac{\theta_l}{1 - \theta} \right. \\ &\quad \left. - \left[ \theta_l - \frac{(2\sqrt{\lambda} - 1)^2 \theta_s^2 \theta_l}{(1 - \theta_s)^2} + \frac{2(2\sqrt{\lambda} - 1)^2 \theta_s^2}{1 - \theta_s} \right. \right. \\ &\quad \left. \left. + 2(2\sqrt{\lambda} - 1)\theta_s \right] \frac{\theta_l}{(1 - \theta)^2} \right\},\end{aligned}\quad (10)$$

where  $\theta = \theta_s + \theta_l$  and

$$\begin{aligned}\phi_l^0(\theta_s) = \bar{j}_0 &= (1 - \theta_s) \exp \left\{ - \frac{(4\lambda - 1)\theta_s}{1 - \theta_s} \right. \\ &\quad \left. - \left[ \frac{(2\sqrt{\lambda} - 1)\theta_s}{1 - \theta_s} \right]^2 \right\}\end{aligned}\quad (11)$$

is the ASF function of larger particles for  $\theta_l = 0$  and  $\bar{j}_0$  can be treated as the dimensionless adsorption flux of larger particles at surfaces precovered with smaller particles.

The low coverage expansion of Eq. (10) up to the second order of  $\theta_l$  is

$$\frac{\phi_l}{\phi_l^0} = 1 - C'_1(\theta_s) \theta_l + C'_2(\theta_s) \theta_l^2 + 0(\theta_l^3), \quad (12)$$

where the constants  $C'_1$  and  $C'_2$  are

$$\begin{aligned}C'_1 &= \frac{4 + (4\lambda + 4\sqrt{\lambda} - 7)\theta_s + 2(2\sqrt{\lambda} - 1)^2 \theta_s^2 / (1 - \theta_s)}{(1 - \theta_s)^2}, \\ C'_2 &= \frac{a(\theta_s)}{(1 - \theta_s)^3} + \frac{a^2(\theta_s)}{2(1 - \theta_s)^4} + \frac{b(\theta_s)}{(1 - \theta_s)^2},\end{aligned}\quad (13)$$

$$a(\theta_s) = 3 + 2(2\lambda + 2\sqrt{\lambda} - 3)\theta_s + 2(2\sqrt{\lambda} - 1)^2 \frac{\theta_s^2}{1 - \theta_s},$$

$$b(\theta_s) = - \left[ 4 + \theta_s \frac{4\lambda + 8\sqrt{\lambda} - 5}{1 - \theta_s} + 3 \left( \frac{(2\sqrt{\lambda} - 1)\theta_s}{1 - \theta_s} \right)^2 \right].$$

By neglecting the  $\theta_l^2$  term one can formally convert Eq. (12) to the quasi-Langmuirian form, i.e.,

$$\frac{\phi_l}{\phi_l^0} = 1 - \frac{\theta_l}{\theta_{\text{mx}}}, \quad (14)$$

where

$$\theta_{\text{mx}} \cong \frac{1}{4 + (4\lambda + 4\sqrt{\lambda} - 7)\theta_s}. \quad (15)$$

The advantage of this formulation over the semiempirical Langmuir model widely used in the literature is that  $\theta_{\text{mx}}$  values can be calculated *a priori* for a given coverage of smaller particles.

## RESULTS AND DISCUSSION

Using the above RSA algorithm extensive calculations were performed for determining both the ASF functions of larger particles, their adsorption kinetics, jamming coverages, and the structure of adsorbed layer.

The quantity of considerable practical interest is the  $\phi_l^0(\theta_s)$  function which represents the averaged probability of adsorbing larger particle over a surface precovered by smaller particles (characterized by the coverage  $\theta_s$ ) normalized to the probability of adsorbing the particle over an uncovered surface. In Fig. 1 the dependence of  $\phi_l^0$  on  $\theta_s$  is plotted for  $\lambda = 1$  (reference curve for monodisperse spheres), 2.2, 5, and 10, respectively. As can be noticed, adsorption probability of larger particles is considerably decreased by the presence of adsorbed small particles, especially for higher  $\lambda$  values. Note that the available experimental data<sup>15</sup> seem to be in a good agreement with the RSA simulations for  $\lambda = 2.2$ .

It is also interesting to observe that the analytical SPT results represented by Eq. (11) reflect well the characteristic features of the  $\phi_l^0$  function. The agreement between the RSA simulations and these analytical predictions seems quantitative when  $\phi_l^0 > 0.1$ . As expected the deviation between equi-

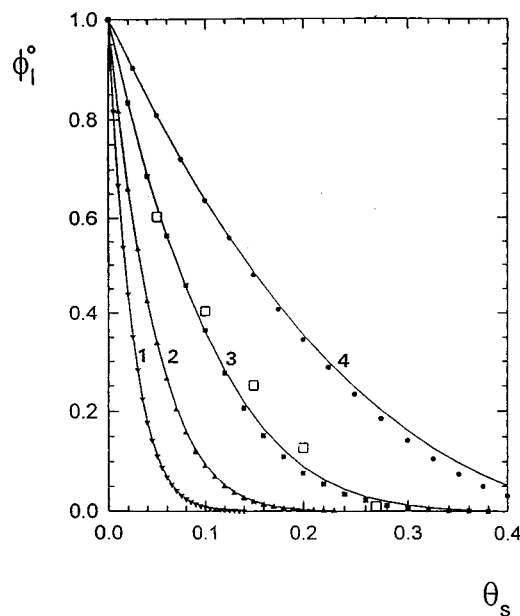


FIG. 1. The dependence of  $\phi_l^0$  on surface concentration of smaller particles  $\theta_s$ . The points denote numerical simulations performed for: (1)  $\lambda=10$ , (2)  $\lambda=5$ , (3)  $\lambda=2.2$ , (4)  $\lambda=1$  (reference, monodisperse system). The continuous lines denote the equilibrium SPT results calculated from Eq. (11) and empty squares represent the experimental results obtained for bimodal suspension of polymeric colloid particles Ref. 15.

librium and RSA results increased for higher  $\theta_s$  values when  $\phi_l^0$  became considerably smaller than 0.1. One may, therefore, conclude that the presence of trace amounts of smaller (e.g., colloid type) particles, hardly detectable by conventional means, should exert a profound effect on adsorption of larger particles (cf. curve 1 in Fig. 1 obtained for  $\lambda=10$ ).

The result shown in Fig. 1 suggest also that the SPT results can be used for practical purposes as a good estimate of  $\phi_l^0$  (initial flux) on precovered surfaces.

Similar, although considerably more time-consuming calculations were performed to determine the dependence of the  $\phi_l$  function on the concentration of larger particles  $\theta_l$  for fixed  $\theta_s$  values. The results obtained for  $\lambda=2.2$  are plotted in Fig. 2. One can observe that the presence of smaller particles considerably reduces  $\phi_l$  which can be well described by the analytical predictions stemming from Eq. (10). However, some positive deviations of the SPT results from the RSA appeared for  $\theta_s > 0.2$ . Since the  $\phi_l$  function assumes small values for this range of  $\theta_s$  the differences are difficult to observe. Analogous calculations performed for  $\lambda=10$  are plotted in Fig. 3.

As can be seen in Figs. 2–3, the deviations of the SPT results from the RSA calculations become quite significant for higher  $\theta_s$ , especially for  $\lambda=10$ . However, for smaller  $\theta_s$  the SPT results can be accepted as a reasonable estimate of  $\phi_l$ .

By knowing the ASF function one can determine the irreversible adsorption kinetics of larger particles from the defining integral

$$\theta_l = k_a c_l S_g \int \phi_l dt = \int \phi_l d\tau, \quad (16)$$

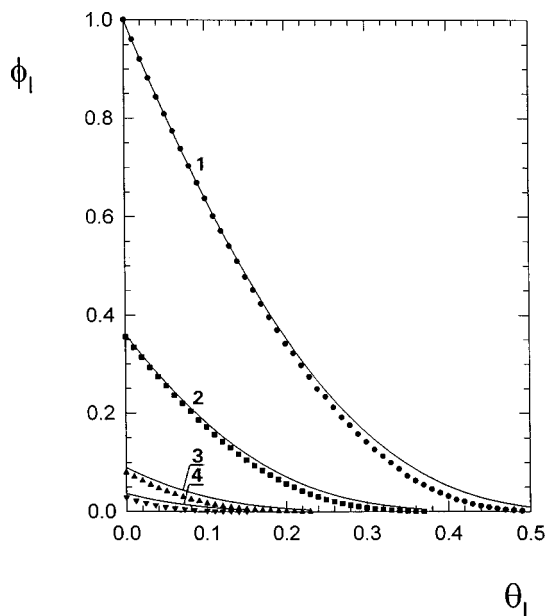


FIG. 2. The dependence of the  $\phi_l$  function of larger particles on  $\theta_l$  calculated numerically for  $\lambda=2.2$  and (1)  $\theta_s=0$ , (2)  $\theta_s=0.10$ , (3)  $\theta_s=0.20$ , (4)  $\theta_s=0.25$ . The continuous lines denote the equilibrium SPT results calculated from Eq. (10).

where  $k_a = j_0/c_l$  is the adsorption constant,  $c_l$  is the bulk concentration of larger particles,  $S_g$  is the characteristic area (usually the particle cross-section area),  $t$  is the dimensional adsorption time and  $\tau = k_a c_l S_g t$  is the dimensionless adsorption time.

As demonstrated previously<sup>11</sup> this dimensionless time corresponds to that used in numerical simulations defined by Eq. (1).

Equation (16) can be used when  $\phi_l$  is known analytically, e.g., for the SPT or quasi-Langmuir model. In the latter

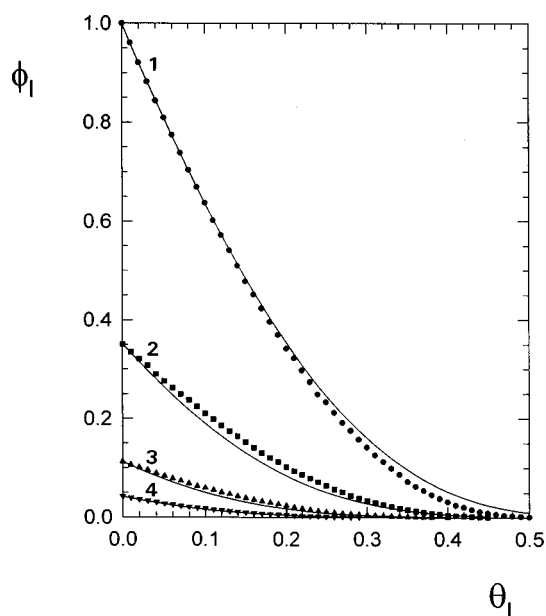


FIG. 3. Same as for Fig. 2 but for  $\lambda=10$ . (1)  $\theta_s=0$ , (2)  $\theta_s=0.025$ , (3)  $\theta_s=0.050$ , (4)  $\theta_s=0.070$ . The continuous lines denote the equilibrium SPT results calculated from Eq. (10).

case the integral can be evaluated explicitly giving the simple expression

$$\theta_l = \theta_{\text{mx}} \left[ 1 - \exp \left( - \frac{\phi_l^0}{\theta_{\text{mx}}} \tau \right) \right] \quad (17)$$

with  $\theta_{\text{mx}}$  defined by Eq. (15) and  $\phi_l^0$  by Eq. (11).

In the case when  $\phi_l$  is known numerically the use of Eq. (16) is less efficient in comparison with direct numerical simulations of adsorption kinetics according to the algorithm described above.

In Figs. 4 the kinetic curves, i.e., the  $\theta_l$  vs  $\tau$  dependencies, are plotted for  $\lambda = 2.2$  and  $\lambda = 10$  (part “b”) derived from the numerical simulations for various surface concentration  $\theta_s$ . The analytical results calculated from the quasi-Langmuirian model, i.e., Eq. (17) are also shown for comparison. As can be seen the quasi-Langmuirian model can be used as a reasonable estimate of adsorption kinetics on precovered surfaces for adsorption times  $\tau < 1$  (the range of validity of this model seems to increase with  $\theta_s$ ). For longer times one can observe, however, systematic deviations of the simulated  $\theta_l$  values from the apparent saturation coverages  $\theta_{\text{mx}}$ .

In order to compress the infinite time domain into a finite one  $\tau^{-1/2}$  was used as the independent variable for  $\tau > 4$  (right-hand side of Figs. 4). This transformation was successfully applied previously<sup>3-5</sup> for presenting the RSA results for uncovered surfaces when

$$\theta_{\infty} - \theta_l \sim \tau^{-1/2}, \quad (18)$$

where  $\theta_{\infty}$  is the jamming coverage for monodisperse spheres calculated to be 0.547.<sup>9</sup>

Thus when plotting  $\theta_l$  vs  $\tau^{-1/2}$ , a straight line dependence should be obtained. As can be observed in Figs. 4 this seems to be the case for adsorption at precovered surfaces. However, the range of the asymptotic regime characterized by the power-law dependence of  $\theta_l$  on  $\tau$  was decreased considerably with the increase in  $\theta_s$ .

The occurrence of these asymptotic regimes implies, therefore, that for longer adsorption times isolated targets existed only whose size distribution was uniform.<sup>3</sup>

One can also deduce that the  $\theta_l$  vs  $\tau^{-1/2}$  dependence implies that the ASF function for the asymptotic regime should assume the form

$$\phi_l \sim [\theta_l^{\infty}(\theta_s) - \theta_l]^3, \quad (19)$$

where the jamming coverages  $\theta_l^{\infty}$  are dependent on the initial coverage of smaller particles.

In our calculations these jamming concentrations were obtained by the linear fitting of the  $\theta_l$  vs  $\tau^{-1/2}$  dependencies and subsequent extrapolation to  $\tau^{-1/2} = 0$  ( $\tau \rightarrow \infty$ ). Averages from five independent computer runs were taken in order to attain a sufficient precision of  $\theta_l^{\infty}$ . These data are compiled in Table I for  $\lambda = 2.2, 5$ , and 10.

The dependencies of the jamming concentrations  $\theta_l^{\infty}$  on  $\theta_s$  are also shown graphically in Fig. 5. For sake of convenience the total coverage, i.e., the sum  $\theta_s + \theta_l^{\infty}$  is also plotted in Fig. 5. The characteristic feature of the  $\theta_l^{\infty}$  vs  $\theta_s$  dependencies is that they fall abruptly to very small values when  $\theta_s$  is increased.

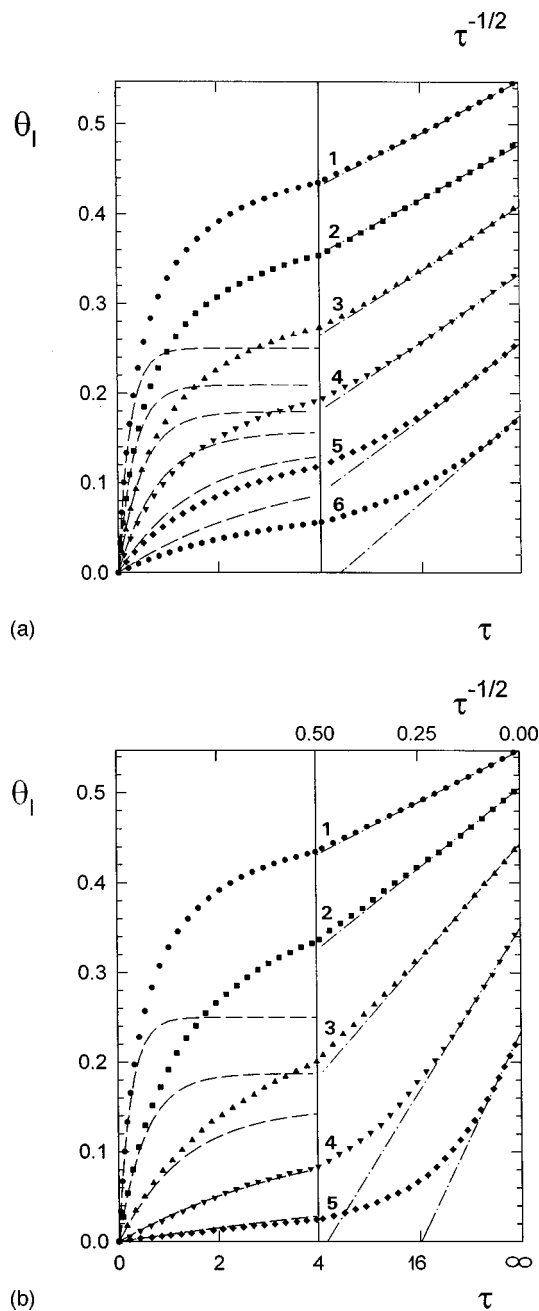


FIG. 4. Kinetics of larger particle adsorption at surfaces precovered with smaller particles expressed as  $\theta_l$  vs  $\tau$  dependencies; (a)  $\lambda = 2.2$  (1)  $\theta_s = 0$ , (2)  $\theta_s = 0.05$ , (3)  $\theta_s = 0.10$ , (4)  $\theta_s = 0.15$ , (5)  $\theta_s = 0.20$ , (6)  $\theta_s = 0.25$ . The broken lines denote the analytical results calculated from Eq. (17) and the -.- lines denote the linear fits, i.e.,  $\theta_l^{\infty} - \theta_l \sim \tau^{-1/2}$ . (b) same as for (a) but for  $\lambda = 10$  and (1)  $\theta_s = 0$ , (2)  $\theta_s = 0.025$ , (3)  $\theta_s = 0.05$ , (4)  $\theta_s = 0.07$ , (5)  $\theta_s = 0.10$ .

It has been found that the numerical results can well be fitted by the interpolating functions (cf. solid lines in Fig. 5)

$$\theta_l^{\infty} = \theta_{\infty} [c/(c - \theta_s)]^2, \quad (20)$$

where  $c$  are the dimensionless constants equal 0.596 for  $\lambda = 2.2$ ; 0.404 for  $\lambda = 5$  and 0.274 for  $\lambda = 10$ .

On the other hand, in the low coverage limit, i.e., for  $\theta_l^{\infty} < 0.1$  the character of the numerical data can better be reflected by the interpolating function

TABLE I. Jamming concentration of larger spheres  $\theta_l^\infty$  at precovered surfaces.

| $\theta_s$      | $\theta_l^\infty$    | $\theta_l^\infty + \theta_s$ |
|-----------------|----------------------|------------------------------|
| $a_l/a_s = 2.2$ |                      |                              |
| 0.0000          | 0.5470               | 0.5470                       |
| 0.0500          | $0.4762 \pm 0.0026$  | 0.5262                       |
| 0.1000          | $0.4079 \pm 0.0022$  | 0.5079                       |
| 0.1500          | $0.3326 \pm 0.0033$  | 0.4826                       |
| 0.2000          | $0.2550 \pm 0.0054$  | 0.4550                       |
| 0.2500          | $0.1750 \pm 0.0020$  | 0.4250                       |
| 0.3000          | $0.0900 \pm 0.0030$  | 0.3900                       |
| 0.3200          | $0.0604 \pm 0.0008$  | 0.3804                       |
| 0.3400          | $0.0378 \pm 0.0017$  | 0.3778                       |
| 0.3600          | $0.0193 \pm 0.0017$  | 0.3793                       |
| 0.3800          | $0.0080 \pm 0.0010$  | 0.3880                       |
| 0.4000          | $0.0024 \pm 0.0007$  | 0.4025                       |
| $a_l/a_s = 5$   |                      |                              |
| 0.0000          | 0.5470               | 0.5470                       |
| 0.0500          | $0.4735 \pm 0.00018$ | 0.5235                       |
| 0.1000          | $0.3680 \pm 0.0009$  | 0.4680                       |
| 0.1500          | $0.2249 \pm 0.0015$  | 0.3749                       |
| 0.1700          | $0.1640 \pm 0.0020$  | 0.3340                       |
| 0.2000          | $0.0832 \pm 0.0023$  | 0.2832                       |
| 0.2200          | $0.0455 \pm 0.0011$  | 0.2655                       |
| 0.2400          | $0.0206 \pm 0.0008$  | 0.2606                       |
| 0.2500          | $0.0137 \pm 0.0012$  | 0.2637                       |
| 0.2600          | $0.0082 \pm 0.0007$  | 0.2682                       |
| 0.2700          | $0.0049 \pm 0.0005$  | 0.2749                       |
| $a_l/a_s = 10$  |                      |                              |
| 0.0000          | $0.5470 \pm 0.0021$  | 0.5470                       |
| 0.0200          | $0.5134 \pm 0.0021$  | 0.5334                       |
| 0.0400          | $0.4704 \pm 0.0021$  | 0.5104                       |
| 0.0600          | $0.4080 \pm 0.0020$  | 0.4680                       |
| 0.0800          | $0.3302 \pm 0.0016$  | 0.4102                       |
| 0.0900          | $0.2830 \pm 0.0017$  | 0.3730                       |
| 0.1000          | $0.2341 \pm 0.0024$  | 0.3341                       |
| 0.1100          | $0.1800 \pm 0.0030$  | 0.2900                       |
| 0.1200          | $0.1350 \pm 0.0040$  | 0.2550                       |
| 0.1300          | $0.0944 \pm 0.0009$  | 0.2244                       |
| 0.1400          | $0.0620 \pm 0.0050$  | 0.2020                       |
| 0.1500          | $0.0384 \pm 0.0021$  | 0.1884                       |
| 0.1600          | $0.0208 \pm 0.0004$  | 0.1808                       |
| 0.1700          | $0.0110 \pm 0.0010$  | 0.1810                       |
| 0.1800          | $0.0060 \pm 0.0010$  | 0.1860                       |

$$\theta_l^\infty = c\lambda\phi_l^0(\theta_s), \quad (21)$$

where  $\phi_l^\infty(\theta_s)$  is the ASF function given by Eq. (11) and  $c$  are the dimensionless constants equal explicitly 3.78 for  $\lambda = 2.2$ ; 6.67 for  $\lambda = 5$  and 9.3 for  $\lambda = 10$ . Another interesting feature of the data shown in Fig. 5 is that the net surface coverage of adsorbed particles passes through a minimum whose depth increased considerably for larger  $\lambda$ . The minimum coverages were found to be 0.378 for  $\lambda = 2.2$  ( $\theta_s = 0.34$ ) 0.261 for  $\lambda = 5$  ( $\theta_s = 0.24$ ) and 0.181 for  $\lambda = 10$  ( $\theta_s = 0.16$ ). These results represent a spectacular manifestation of the irreversibility effect since the composition and density of “monolayers” formed by particles is dependent on the peculiarities of the adsorption path, e.g., order of bringing particles to the interface. Physically, this can be realized by replacing the smaller particle suspension after a given adsorption time by the larger particle suspension.

This effect is also demonstrated in Figs. 6(a)–6(c) where various monolayers under the jamming state are shown (simulated numerically for  $\lambda = 2.2$  and  $\tau = 10^4$ ). Depending

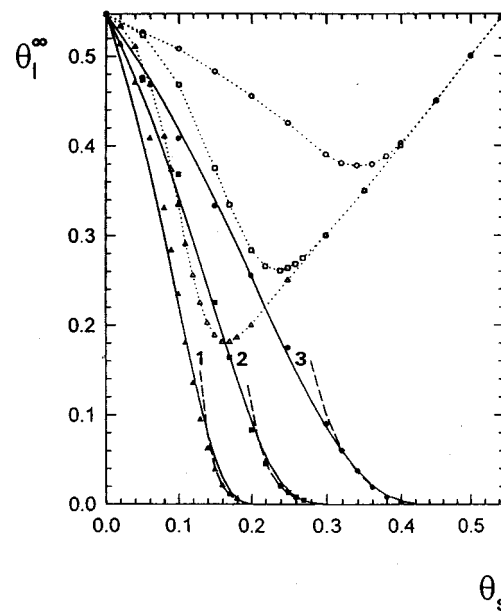


FIG. 5. The dependence of the jamming concentration of larger particles  $\theta_l^\infty$  on surface concentration of smaller particles  $\theta_s$ ; the points (full symbols) denote results of numerical simulations performed for (1)  $\lambda = 10$ , (2)  $\lambda = 5$ , (3)  $\lambda = 2.2$ . The empty symbols represent the net coverage, i.e.,  $\theta_l^\infty + \theta_s$ , the continuous lines represent the fitting functions given by Eq. (20) and the broken lines show the limiting results calculated from Eq. (21).

on the initial value of  $\theta_s$ , a complete jamming was attained for the total coverage ranging between 0.39 [Fig. 6(a)] and 0.51 [Fig. 6(c)].

The distributions of larger particles shown in Figs. 6 seem also qualitatively different from analogous distributions (at the same coverage) observed previously for monodisperse systems.<sup>11</sup> This was demonstrated quantitatively by determining the radial distribution function of larger particles  $g_l$  according to the method described above. The results are shown in Figs. 7(a)–7(c) for  $\theta_l$  equal 0.09, 0.25 and 0.41, respectively. For comparison the  $g_l$  function determined from numerical simulations for a monodisperse system at the same surface coverage is also plotted in Figs. 7. As can be seen, for the bimodal system at low coverages, the shape of the radial distribution function deviates significantly from its monodisperse counterpart, especially for low coverages  $\theta_l$ . Thus for  $\theta_l = 0.09$  of Fig. 7(a) a well-pronounced depletion zone can be observed (for  $2 < r/a_l < 2.6$ ) followed by a maximum of a considerable height. By contrast, for monodisperse system the  $g_l$  function decreased monotonically for this range of distances. It is interesting to note that the shape of the  $g_l$  function for bimodal systems is quite analogous to the radial distribution functions predicted theoretically and observed experimentally for monodisperse systems of electrostatically interacting particles.<sup>11</sup>

However, in the case of bimodal systems the depletion zone effect is caused by the fact that larger particle adsorption occurs mostly at isolated targets separated from each other by distances comparable with the smaller particle diameter.

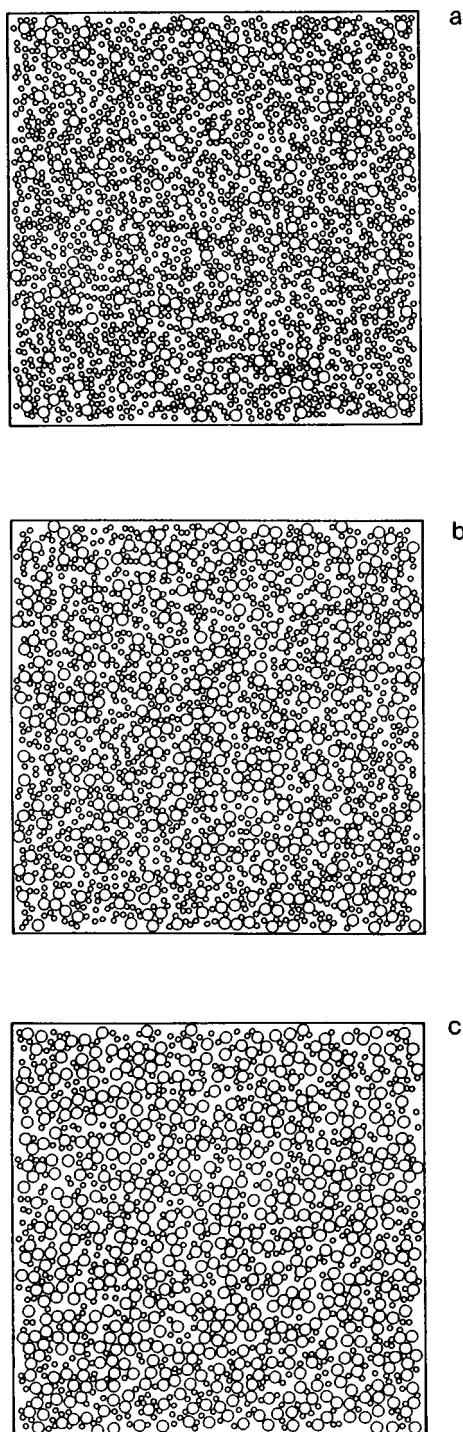


FIG. 6. The adsorbed particle "monolayers" close to the jamming limit simulated numerically for  $\lambda=2.2$ . (a)  $\theta_s=0.3$ ,  $\theta_l=0.09$ . (b)  $\theta_s=0.2$ ,  $\theta_l=0.25$ . (c)  $\theta_s=0.1$ ,  $\theta_l=0.41$ .

The results shown in Figs. 7 suggest that from the shape of the  $g_l$  function of larger particles important information can be extracted concerning the concentration and the size of preadsorbed particles.

## CONCLUDING REMARKS

It was found that the numerical RSA simulations concerning adsorption at precovered surfaces can well be approximated in the limit of low densities by the extrapolated

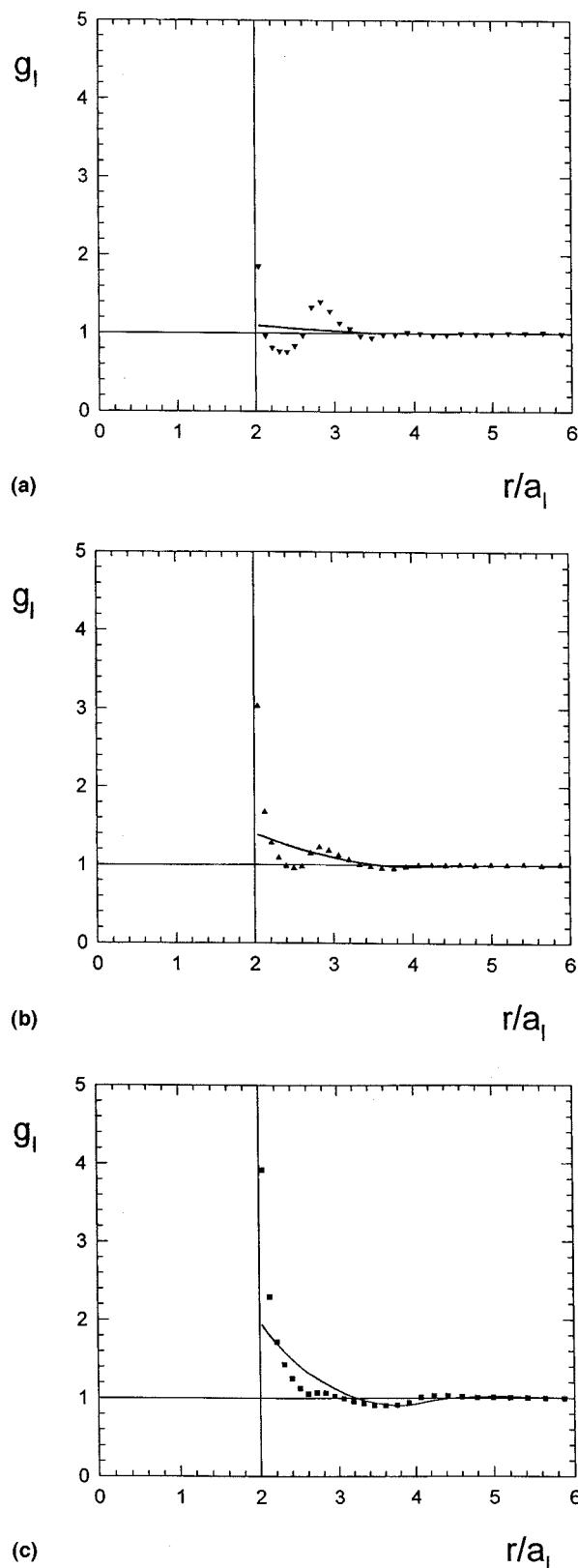


FIG. 7. The pair correlation function of larger particles  $g_l$  derived from numerical simulations for  $\lambda=2.2$ . (a)  $\theta_s=0.3$ ,  $\theta_l=0.09$ . (b)  $\theta_s=0.2$ ,  $\theta_l=0.25$ . (c)  $\theta_s=0.1$ ,  $\theta_l=0.41$ . The continuous lines denotes the smoothed results obtained for monodisperse systems characterized by the same  $\theta_l$ .

SPT theory with the geometrical parameter  $\gamma=2\sqrt{a_l/a_s}-1$  instead of  $a_l/a_s$  for disks (2D case). As a direct manifestation of irreversibility it was also shown that the total jamming coverage of bimodal mixtures passes through a mini-



mum whose depth may become considerable for larger  $\lambda$  values. These theoretical predictions derived from the RSA simulations suggest that both the adsorption kinetic (initial flux) and the jamming coverages of particles are very sensitive to the presence at interfaces of trace amounts of smaller sized particles often difficult to detect by conventional analytical means. These theoretical prediction may explain the persisting difficulties in obtaining reliable kinetic data and monolayer densities in protein adsorption processes being usually of an irreversible character.

In comparison with monodisperse systems, adsorption at precovered surfaces is leading to different structures, characterized in terms of the radial distribution function. Hence, by determining  $g_l$  for larger particles important clues about the presence of smaller sized preadsorbed particles (contaminants) can be drawn.

## ACKNOWLEDGMENT

This work was partially supported by the KBN Grant No. 3T09 A08310.

- <sup>1</sup>A. Renyi, Publ. Math. Inst. Hung. Acad. Sci. **3**, 109 (1958).
- <sup>2</sup>J. J. Gonzales, P. C. Hemmer, and J. S. Hoye, Chem. Phys. **3**, 288 (1974).
- <sup>3</sup>E. L. Hinrichsen, J. Feder, and T. Jossang, J. Stat. Phys. **44**, 793 (1986).
- <sup>4</sup>P. Schaaf and J. Talbot, J. Chem. Phys. **91**, 4401 (1989).
- <sup>5</sup>J. Talbot, G. Tarjus, and P. Schaaf, Phys. Rev. A **4**, 4808 (1989).
- <sup>6</sup>S. M. Ricci, J. Talbot, G. Tarjus, and P. Viot, J. Chem. Phys. **97**, 5219 (1992).
- <sup>7</sup>J. Talbot, P. Schaaf, and G. Tarjus, Mol. Phys. **72**, 1397 (1991).
- <sup>8</sup>Z. Adamczyk and P. Weroński, J. Chem. Phys. **105**, 5562 (1996).
- <sup>9</sup>J. W. Evans, Rev. Mod. Phys. **65**, 1281 (1993).
- <sup>10</sup>J. J. Ramsden, Phys. Rev. Lett. **71**, 295 (1993).
- <sup>11</sup>Z. Adamczyk, B. Siwek, M. Zembala, and P. Belouschek, Adv. Colloid Interface Sci. **48**, 151 (1994).
- <sup>12</sup>J. Talbot, and P. Schaaf, Phys. Rev. A **40**, 422 (1989).
- <sup>13</sup>P. Meakin, and R. Jullien, Phys. Rev. A **46**, 2029 (1991).
- <sup>14</sup>Z. Adamczyk, B. Siwek, M. Zembala, and P. Weroński, J. Colloid Interface Sci. **185**, 236 (1997).
- <sup>15</sup>Z. Adamczyk, B. Siwek, and P. Weroński, J. Colloid Interface Sci. **195**, 261 (1997).
- <sup>16</sup>H. Reiss, H. L. Frisch, and J. L. Lebowitz, J. Chem. Phys. **31**, 369 (1959).
- <sup>17</sup>J. L. Lebowitz, E. Helfand, and E. Praestgaard, J. Chem. Phys. **43**, 774 (1965).
- <sup>18</sup>J. Talbot, X. Jin, and N. H. L. Wang, Langmuir **10**, 1663 (1994).
- <sup>19</sup>B. Widom, J. Chem. Phys. **44**, 3888 (1966).